Towards Strength–Ductility Synergy through the Synthesis and Processing of a Hybrid Sustainable AHSS, XHSS, and UHSS

Mahmoud M Abu Elkhier[1], Bakr M Rabeeh[3], S kaitbay[2] and Amir A Abdelsalam[2]

[1] Ph.D. Postgraduate, Benha College of Engineering, Benha University, Egypt
[2] Staff members, Benha College of Engineering, Benha University, Egypt
[3] Professor of Engineering, German University in Cairo (GUC)
Corresponding author: mahmoud.abuelkhier@gmail.com

Abstract. Steel can be processed to reach ultra-high strength through a complicated, energy consuming time, heat treatment but usually at a drastic loss of ductility. By purposely deploying, a thermomechanical processing for heterogeneous nanostructures in an otherwise single or dual - phase steels. A ceramization, powder pack processing is being used with eutectic Boron mixture along with ammonium bicarbonate. A non-traditional hybrid structure is being introduced as a recent advance in overcoming this trade-off. Several structural designs are being explored, however a sandwich, and hierarchical, functionally gradient, domain-dispersed nanostructures is being introduced. A distinct comparison is being achieved in low alloy steel (A333 grade 6) and high alloy austenitic Mn-steel (S-52) normalized achieving either advanced high strength steel (AHSS), advanced extra-high strength steel (A-XHSS), or advanced ultra-high strength steel (A-UHSS).Ultra-fast ceramization is conducted at low energy input at 220°C, with time domain (10 and 30 minute). Low melting depressant temperature, LMD, coating (Boron-Mixture, and Ammonium Bicarbonate (ABC)), stress mismatch and thermal gradient are being considered. All previous factors induce intentional structural heterogeneities with alloy segregation, twinning, recrystallization, localized micro-plasticity, along with dominant ductility, and/or precipitated hardened phase. Moreover, these heterogeneous nanostructures in steels at ultra-fast low temperature ceramization (220°C /10 minute) play a significant role similar to multiple phases in complex alloys, for functionally graded hybrid (ceramic/metal) composite structure. A compromising is being achieved via these future innovations (Ceramization) towards a synergetic effect between high strength and high ductility, highlighting several recent steel classes (AHSS, XHSS, and UHSS). The key takeaway for this advanced low temperature processing is not only, a thermomechanical behaviour, but also a thermochemical fusion reaction along with techno economic energy and time saving of the corresponding fabricated part. A good balance of strength and ductility is achieved for either advanced high strength steel with energy balance (X~ 20,000 MPa %), advanced extra high strength steel with energy balance (X~ 40,000 MPa %) or advance ultra-high strength steel with energy balance (X ~ 60,000 MPa %) for either aerospace or automotive engineering, identifying outstanding energy challenges and sustainable opportunities.

Keywords advanced high strength, extra high strength, high ductility, fusion, high strength, hybrid, heterogeneous, thermomechanical, thermochemical, synergy, and ultra-high strength.

1. Introduction

Steel is a structural metal as the workhorse material for the manufacturing industry and structural applications. This is largely because they have a good balance of strength and ductility. There is however a relentless quest to reach a more superior combination of strength and ductility. Unfortunately, these two properties are usually considered mutually exclusive: a gain in strength is inevitably accompanied by a sacrifice in ductility, resulting in a strength–ductility trade-off [1–6]. For example, homogeneous nanocrystalline metals exhibit ultra-high strengths over 1 GPA, but that comes with diminishing (e.g., less than 5%) ductility (defined as the strain to failure in a uniaxial tension test) [7]. The major challenge, therefore, is to engineer novel microstructures to restore a respectable ductility to these high-strength steel, so as to achieve a desirable strength–ductility synergy [8, 9]. There have been many success stories in the intrinsically designed multicomponent and multiphase alloy steel [10, 11], as well as composites [12, 13], to achieve high strength while retaining reasonable ductility.

Elemental and single-phase metals are desirable in many applications [14-18], however or instance, additional components or phases increase variables of processing and cost, make the material prone to corrosion due to inhomogeneities and associated disparity in electrochemical potentials, reduce the electrical and thermal conductivity, and bring in sites for stress concentration and crack initiation. Moreover, precipitation and dispersion of different phases require a delicate control of the phase decomposition sequence (e.g., to avoid over-aging in precipitation hardening). Wu et al. reported the processing of a novel class of heterogeneous nanostructures that involves “self-dispersion strengthening without the second phase” in Ni [18]. Three desirable features of high strength, high strain hardening rate and high ductility are realized simultaneously. In recent years, new material processing routes have emerged that enable microstructural control on the nanometer scale. One can now create heterogeneous nanostructures in an otherwise single-phase steel metal. The progress has exploited this opportunity, through a common design strategy of heterogeneous nanostructured Steel-metals (HNMs) via different traditional heat treatments [19-25]. From this particular standpoint, the primary questions we aim to address are; (i) what kind of nanostructure design in single-phase metals can push the boundary of the strength–ductility combination, and (ii) what the new thermomechanical deformation mechanisms are responsible for the enhanced strength–ductility synergy in these heterogeneous nanostructures. A non-traditional ultra-fast ceramization process is introduced to answer these two questions for the target of a hybrid sandwich structure intrinsically introduced for extrinsically developed strategies of overcoming the strength–ductility synergy for complex advanced high strength steel and functionally graded ceramic-metal composites [26].

Towards strength–ductility Synergy, ultra-fast ceramization is a non-traditional thermomechanical treatment with thermochemical fusion reaction is introduced for intrinsically and extrinsically synthesis and processing a sustainable either advanced, extra, or even ultra-high strength steel (AHSS, XHSS, and/or UHSS). Distinct tactics with a unifying elemental kinetic principle in that; the intentional structural heterogeneities, along with localized melting, alloy segregation, thermochemical fusion, and twinning induce non-homogeneous plastic deformation, recrystallization, thereby enhancing strength and ductility. Moreover, these heterogeneous nanostructures in metals play a role similar to multiple phases in complex alloys, functionally graded materials and composites, sharing common material design and mechanics principles. Ceramization and ultra-fast powder pack boronizing is achieved for either low alloy (A333 Gr6), or a high, austenitic Mn steel (S 52 Normalized), as a future innovation for outstanding conservative

energy challenges and sustainable opportunities. Microstructural evaluation via optical, scanning electron microscopy, with energy dispersive X-ray spectroscopy are conducted along with mechanical characterization tensile and flexural strength testing. Ceramization kinetics, is being considered with surface and bulk hardening, possibility of hybridization, thermomechanical, thermochemical fusion "thermite" reaction, with localized ceramic/metal bonding for outstanding energy challenges and sustainable opportunities, with different outstanding advanced ultra-high strength steel grades.

2. Materials and Processing

During materials design and processing, one needs to control and optimize not only the volume fraction, but also the morphology and topology, of the heterogeneities, as all these variables might strongly influence the properties. The grain size distribution, spatial variation (e.g., constant gradient, varying gradient, random gradient, magnitude of gradient), and morphology (lamellae, domains, aggregates, percolation, etc.) can all be inter-related design parameters that change mechanical properties. To control all of these factors in bulk samples, it is necessary but challenging to invent a novel nontraditional processing method (e.g., gradient is often produced by surface treatment, traditional). In this regard, ceramization, with ultrafast powder pack boronizing is introduced at low miscibility temperature 220℃ for 10 and 30 minutes and considered for a hybrid, functional graded advanced structural materials. Heterogeneities and considerable complexity in structure processing is being considered. It is also a major challenge to reach the designed hybrid, FGM, composite structures. On the bright side, there are many parameters as knobs to turn for achieving the optimal strength–ductility combination. It is worth noting that traditional heat treatment for AHSS, such transformation induced plasticity (TRIP), as well as thermomechanical treatment, twinning induced plasticity (TWIP) are both merged in one innovative ultra-fast ceramization along with thermochemical fusion "thermite" reaction as a techno-economic key takeaway processing.

At the front of microstructure characterization, low alloy steel (A333 Gr.6), and high alloy austenitic Mn-steel (S-52 N) are selected for comparison. Ceramization/boronization is being conducted, mechanically and microstructurally investigated. Tensile tests, and 3-point flexural bending tests are established at room temperature to quantitatively measure the mechanical properties of a representative as-received Mn-Steel, as well as ceramized/boronized steel specimens. In addition, microstructural characterization is being also, conducted via optical microscopy, scanning electron microscopy, and energy dispersive X-ray spectroscopy (EDX). Chemical composition of as-received Mn-Steel, S- 52N, is established and presented in Table 1.

Table 1. Chemical composition of Mn- Steel (S-52N) wt. %

Element	C	Si	Mn	P	S	Cr	Ni	Mo	Al
%	0.209	0.209	1.3	0.0078	0.011	0.131	0.122	0.0043	0.029
Element	Co	Cu	Nb	Ti	V	W	Pb	B	Mg
%	0.027	0.247	<0.004	<0.001	0.012	<0.010	<0.003	0.0034	<0.001
Element	Ta	B	Sn	Zn	As	Ce	Zr	Fe balance	
%	0.018	0.00114	0.025	0.0051	0.027	0.0069	0.0036	97.6	

3. Results and Discussion

3.1. Microstructural Characterization

For clear understanding of the observed superb mechanical properties of the ceramized, and ultra-fast boronized steel samples, microstructural characterization is conducted. The microstructures are studied in detail down to the atomic scale for as received (AR) sample and compared with the boronized samples in either low or high alloy steel. Optical microscopy along with scanning electron microscopy (SEM) and energy dispersive X-ray spectroscopy (EDX) with elemental mapping are conducted. Fig. 1a-b, for low and high steel, present the microstructure of as-received seamless, and S-52 Mn specimens respectively. Figure 1a. reveals clear banding of ferritic -pearlitic aligned grains, while Fig. 1b reveals grain structure exhibits a non-uniform distribution of ultrafine equiaxed grains with an average size of 20 μm and random orientations. Figure 2a-b. Presents optical microscopy of ceramized / boronized low alloy specimens at 220°C for 10 minute, reveals twinning of banding at outer specimen; Figure 2a, and bulk area; Figure 2b.

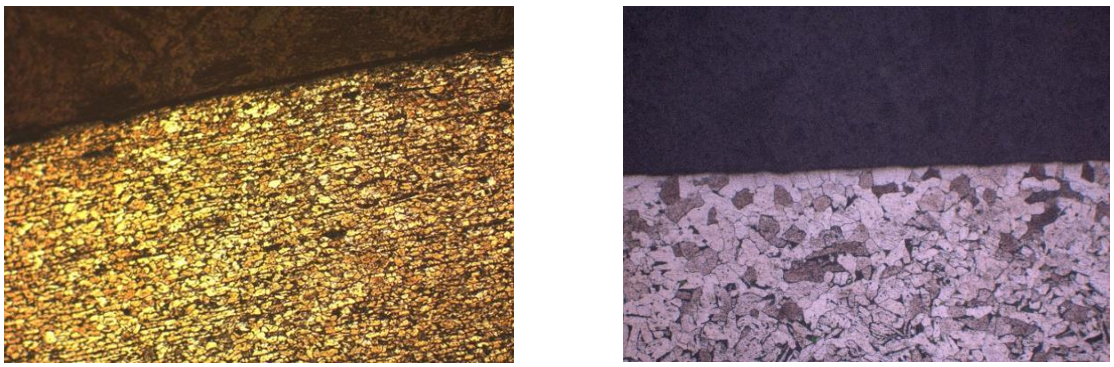

(a) seamless steel (A333. Gr6) with clear banding (b) austenitic Mn-steel (S-52N) with equiaxed grains.

Figure 1. Optical microscopy output for the AR

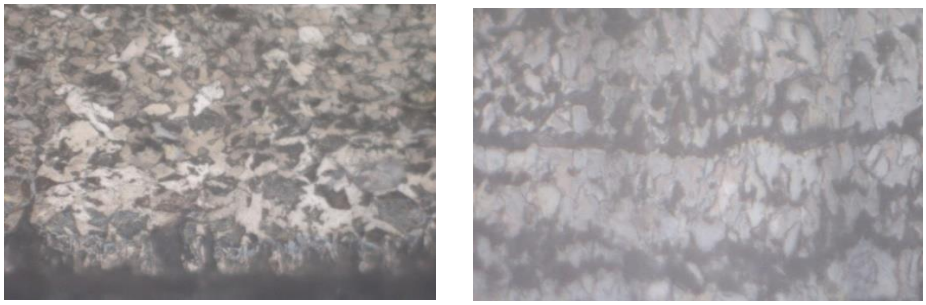

(a) at surface (b) at Bulk center

Figure 2. Optical microscopy of ceramized seamless steel (A333. Gr6) at 220 ^{o}C for 10 min with clear banding and twinning

Figure 3a-b. Represents the optical microscopy of ceramized Mn-alloy steel (S-52N) at 220°C for 30 min with clear (a) boron segregation at the surface, and (b) bulk twinning. While figure 4a-b presents optical microscopy of ceramized/boronized seamless steel (A333 Gr.6), and high alloy specimens (S-52N) at 220°C for 10 and 30 minute respectively. Borate glass steel surface hardened ceramic layer is revealed along with transitionally graded, and twinned structure. Directionality along with grain

boundary alloy segregation and outer grain refinements are dominant with twinning at outer surface at either low alloy or high alloy Mn steel (Figure 4b). Figure 5a-d. Scanning electron microscopy of ceramized Mn-alloy steel (S-52N) at 220°C for 10 min at outer surface with (a) Boron Mix, (b) Boron Mix+ABC, and at (c-d) interface and Bulk material with B Mix+ABC. Fig. 5a reveals black spots of boron segregation intergranular and trans granular with grain flow (commencement of recrystallization). Figure 5b reveals outer surface intergranular micro voids/crack (commencement of defragmentation), Figure 5c reveals outer surface grain-defragmentation in a liquid phase borate glass (B, C) as dark phase. Figure 5d reveals alloy segregation (B, N) induce microstructural changes with sub grains.

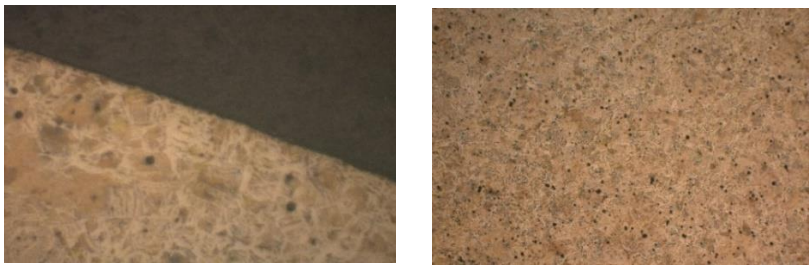

(a) **(b)**

Figure 3. Optical microscopy of ceramized Mn-alloy steel (S-52N) at 220 ºC for 30 min with clear (a) surface boron segregation and (b) Bulk twinning.

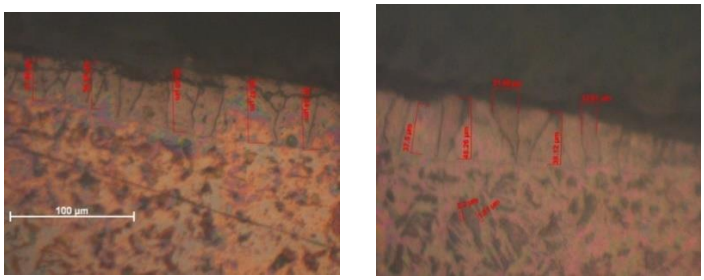

(a) (b)

Figure 4. Optical microscopy of ceramized (a) seamless steel (A333 Gr.6), and (b) Mn-alloy steel (S-52N) at 220 °C for 30 min with clear boron segregation and twinning.

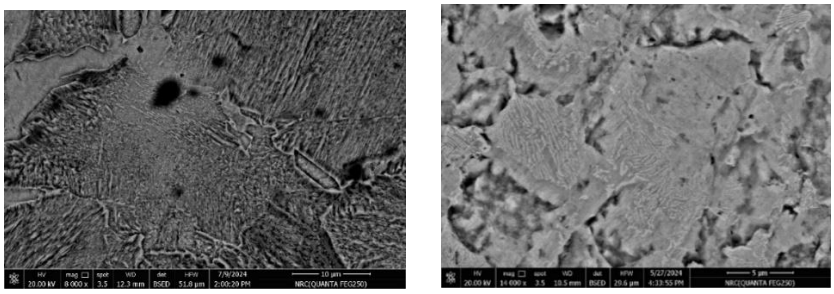

(a) (b)

Figure 5a-b. Scanning electron microscopy of ceramized Mn-alloy steel (S-52N) at 220 °C for 10 min at outer surface with (a) Boron Mix, (b) Boron Mix+ABC

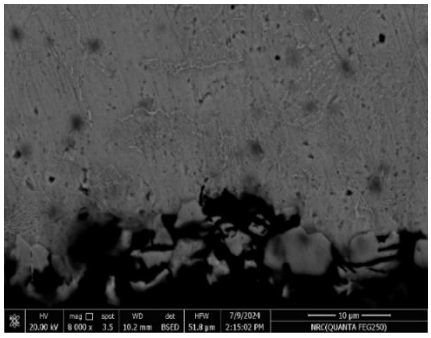

(c)

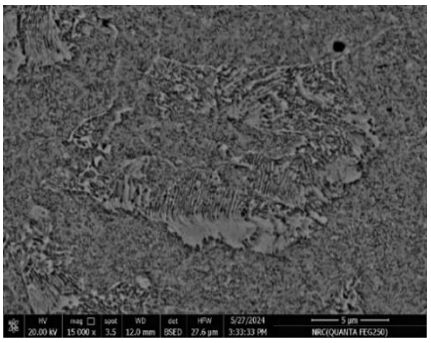

(d)

Figure 5 c-d. Scanning electron microscopy of ceramized Mn-alloy steel (S-52N) at 220 °C for 10 min at outer surface (c), and (d) Bulk material with B Mix+ABC.

Figure 6a-d presents the Scanning electron microscopy of ceramized Mn-alloy steel (S-52N) at 220°C for 30 min with boron Mix at (a) Bulk material, (b) Outer surface, (c) Interface-Thermochemical, and (d) Interface –Thermomechanical meshing. More grain refinements and recrystallization presented in Figure 6a, with more outer surface crystal defragmentation (Figure 6b), with more thermochemical interfacial fusion; Figure 6c, and more thermomechanical interfacial meshing; Figure 6d.

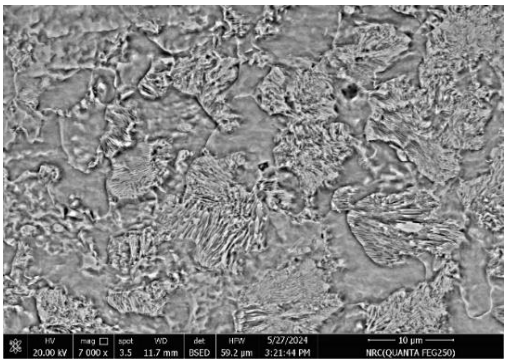

(6-a)

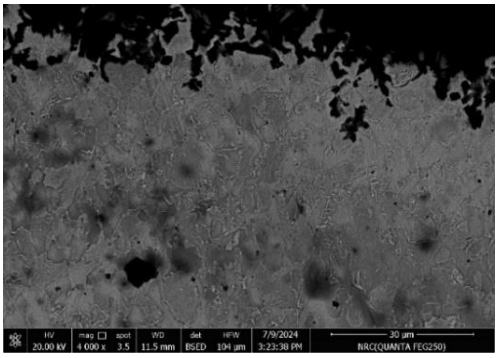

(6-b)

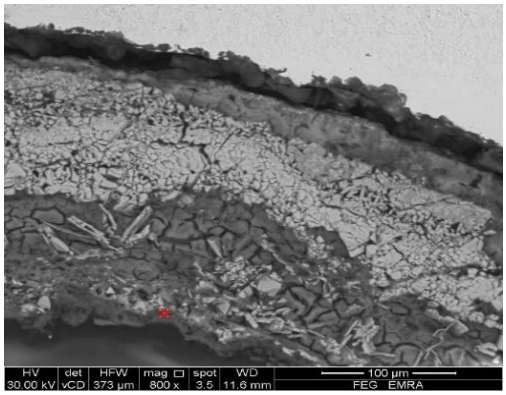

(6-c)

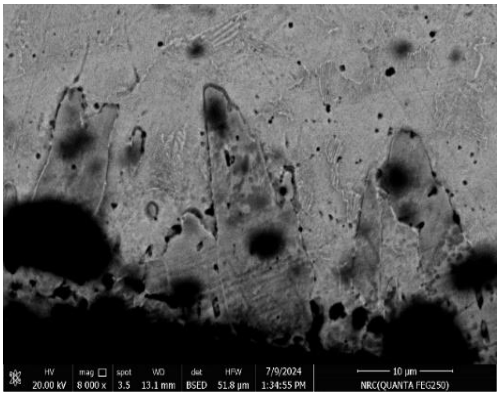

(6-d)

Figure 6 a-d Scanning electron microscopy of ceramized Mn-alloy steel (S-52N) at 220 °C for 30 min with Boron Mix (a) Bulk material, (b) Outer surface, (c) Interface-Thermochemical, and (d) Interface -Thermomechanical.

Figure 7a-d. Shows scanning electron microscopy of ceramized Mn-alloy steel (S-52N) at 220°C for 30 min with Boron Mix and ABC at (a) Bulk material, (b) Outer surface, (c) Interface-Thermochemical, and (d) Interface –Thermomechanical meshing. Alloy segregation along with directionality of grain flow and sub grain refinements and recrystallization presented in Figure 7a, with coherent Nano lamellar (CNL) architectures that exhibit an unprecedented ductility (Figure 7b), more outer surface crystal defragmentation, with more thermochemical interfacial fusion (Figure 7c), and more thermomechanical interfacial meshing; Figure 7d.

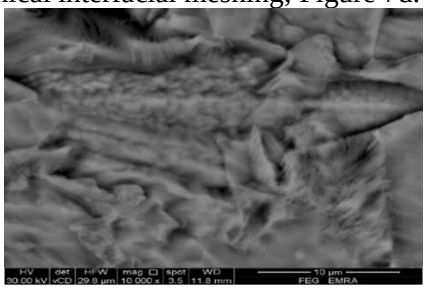

(7-a)

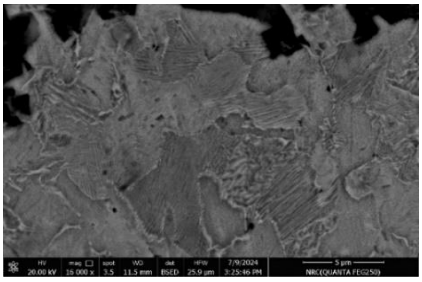

(7-b)

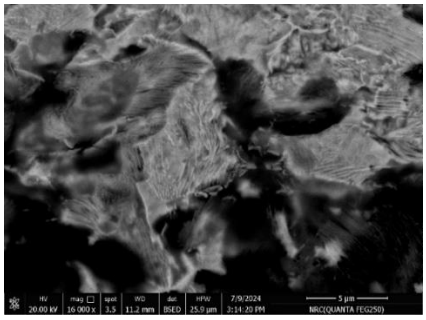

(7-c)

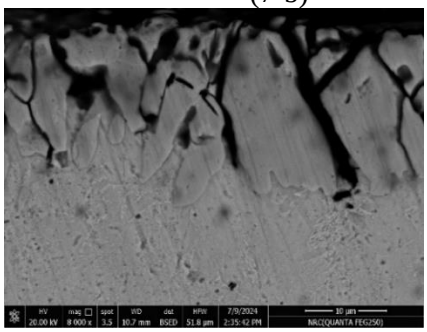

(7-d)

Figure 7a-d Scanning electron microscopy of ceramized Mn-alloy steel (S-52N) at 220 °C for 30 min with Boron Mix+ABC. (a) Bulk material, (b) Outer surface, (c) Interface-Thermochemical, and (d) Interface -Thermomechanical.

Kinetic of ceramization is now captured and presents in Figure 8 a-e. It presents; (a)-Localized melting with alloy segregation; Figure 8a, (b)- phase transformation with stress mismatch; Figure 8b, (c)-thermite reaction with defragmentation; Figure 8c, (d)-twinning and recrystallization; Figure 8d, (e)-chemical and mechanical mesh of ceramic/metal bonding; Figure 8e.

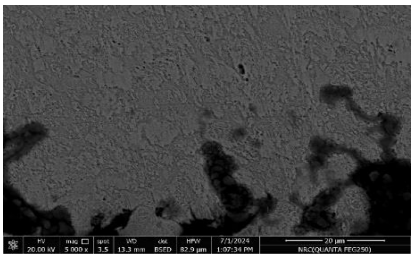

(8-a)-Localized melting with alloy segregation

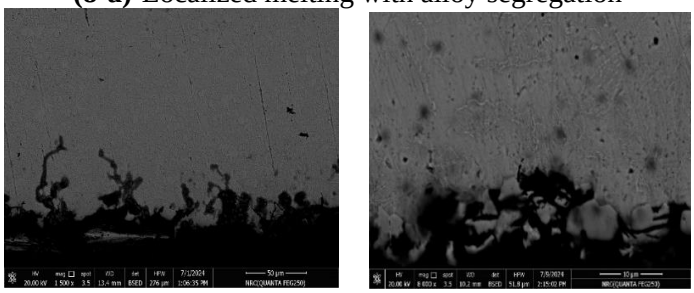

(8-b)- Phase transformation with stress mismatch

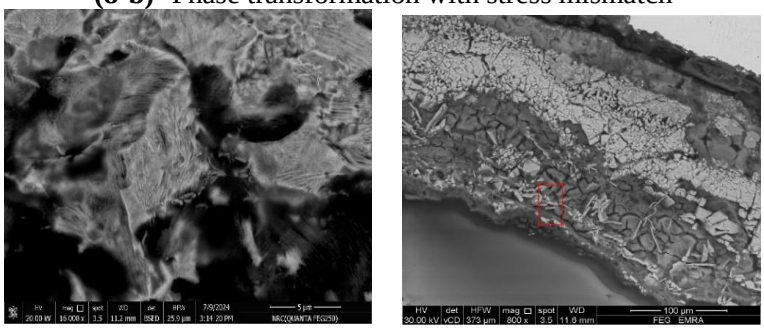

(8-c)-Thermite reaction with defragmentation

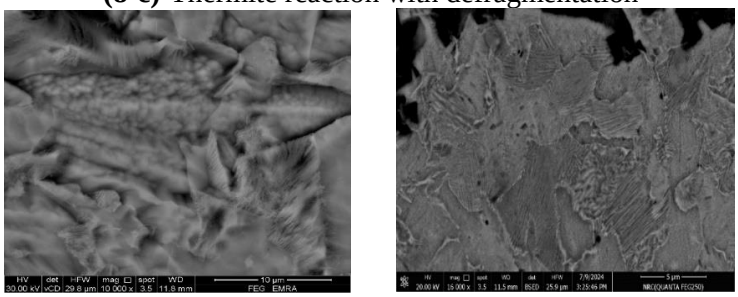

(8-d)-Twinning and recrystallization

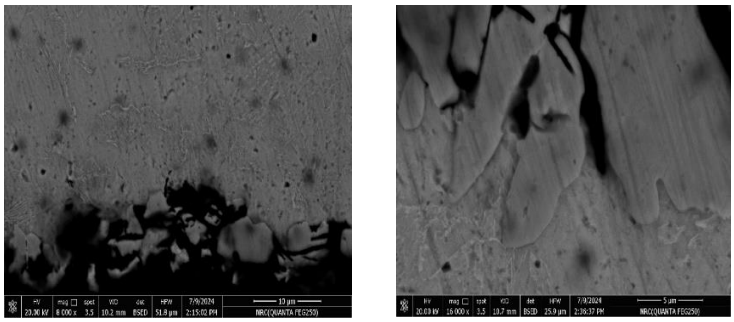

(8-e)- Chemical and mechanical mesh of ceramic/metal bonding

Figure 8a-e Scanning electron microscopy of Kinetic ceramization in Mn-alloy steel (S-52N) at 220 °C for 30 min with Boron Mix+ ABC.

Figure 9a-c. SEM (a) with EDX, areal elemental mapping (b-c) of ceramized Mn-alloy steel (S-2N) at 220°C for 30 min with Boron Mix + ABC. Elemental mapping reveals clear segregation of alloying elements boron, nitrogen, carbon, and aluminum with balance steel. Fig. 10a-d. presents alloy segregation with elemental localized EDX of ceramized Mn-alloy steel (S-52N) at 220°C for 30 min with Boron Mix + ABC. It presents EDX of; (a) Interfacial defragmented steel, (b) Bulk areal steel, (c) Interfacial ceramic/steel (FeB), and (d) Interfacial ceramic/steel (Fe2B). a clear directionality of alloy segregation as boron and nitrogen enter inwards, while Al, C, and Mn depleted and segregate outwards. The defragmented steel is only Fe, and MN, while a clear Al/ steel is localized induce a thermochemical thermite fusion reaction that most interfacial dominant.

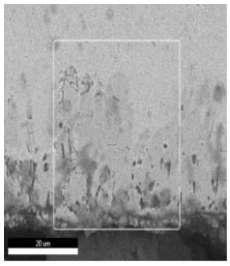

(9-a)

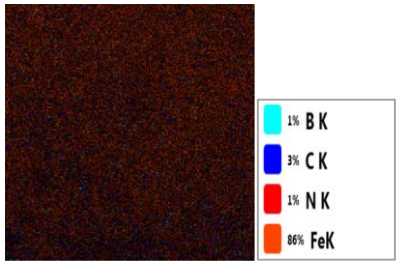

(9-b)

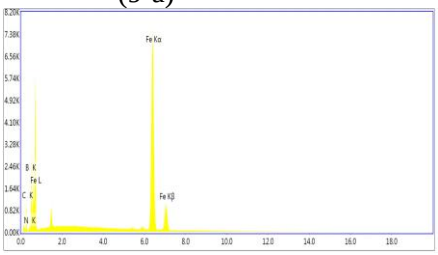

Element	Weight %	Atomic %	Net Int.	Net Int. Error
B K	26.32	50	8.8	0.02
C K	15.35	26.25	19.8	0.01
N K	2.1	3.07	2.9	0.04
FeK	56.23	20.68	468.9	0

(9-c)

Figure 9a-c. SEM (a) with EDX, areal elemental mapping (b-c) of ceramized Mn-alloy steel (S-52N) at 220 °C for 30 min with Boron Mix + ABC

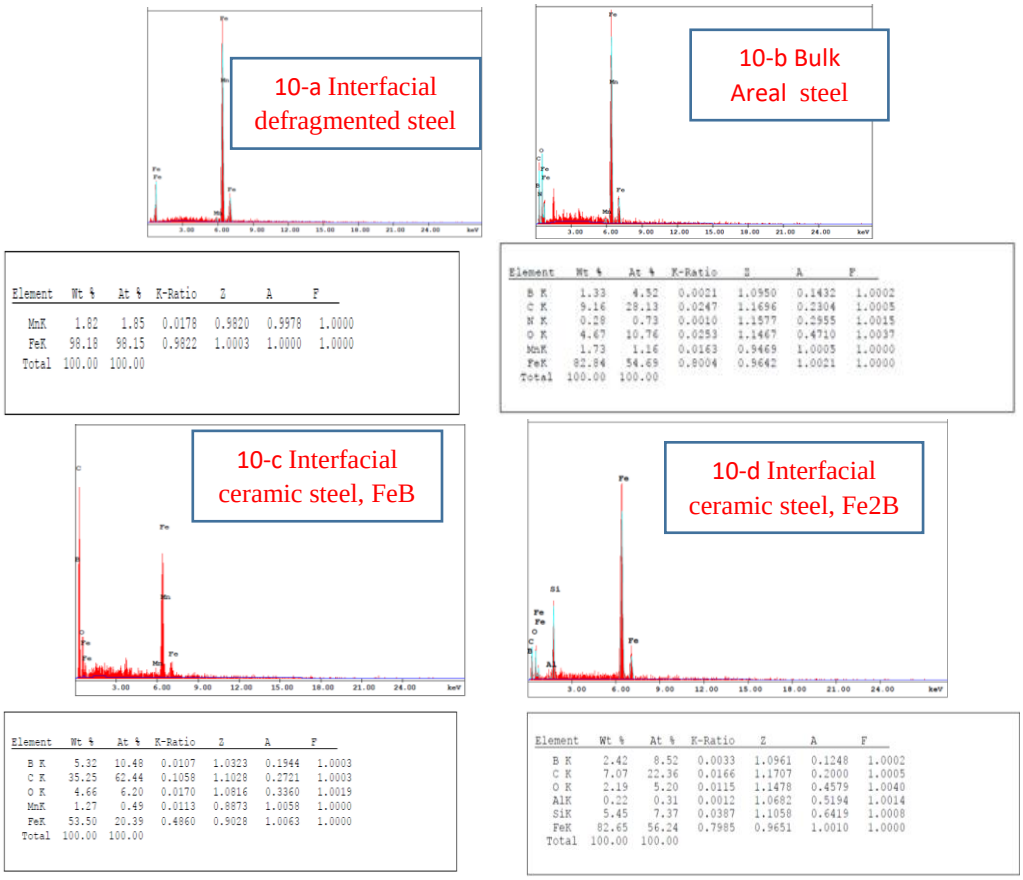

Figure 10a-d. Alloy segregation with Elemental localized EDX of ceramized Mn-alloy steel (S-52N) at 220 °C for 30 min with Boron Mix + ABC

The boronization / ceramization of either low alloy (A333 Gr.6) seamless steel along with austenitic high alloy Mn-steel (S52 N) induce hybrid sandwich structure along with functionally graded ceramic/metal structure with lateral variation of grain refinements along with variation from hard ceramic surface FeB-Fe2B to ductile FCC with CNL structure. Transformation induce plasticity (TRIP) along with twinning induce plasticity (TWIP) are captured. Strengthening mechanisms along with ductility induced persistent slip bands are achieved with a compromised synergetic effect of high strength high ductile structure achieved for advanced extra-high strength steel A-XHSS.

3.2. Mechanical Characterization

Mechanical characterizations are conducted via tensile and 3-point bending flexural strength for monolithic AR and sandwich hybrid/composite samples at room temperature to quantitatively illustrate the mechanical properties. Figure 11a-e. Presents stress-strain diagram of monolithic as received tensile and ceramized seamless steel specimens at 220°C for 10 minutes, with either (Boron Mix) and/or (B Mix +ABC). figure11a reveals low strength for Seamless AR (σ=895.00 MPa, ξ=18.0%), X =16110 MPA. %. Fig. 11b, reveals slightly more increase of strength and ductility when ceramized with Boron Mix only (σ =1003.1 42 MPa, ξ =19.0%), X=19058.9 MPa %. Fig. 11c, reveals slightly more increase of strength and ductility when ceramized with Boron Mix + ABC (σ =1132.42 MPa, ξ =17.5%), X=

19817.35 MPa%, that < AHSS. Fig. 11d, reveals slightly more increase of strength and ductility when ceramized with Boron Mix only (σ =1043.92.42 MPa, ξ =19.0%), X= 19834.48 MPa %. Fig. 11e, reveals slightly more increase of strength and ductility when ceramized with Boron Mix + ABC (σ =1065.64 MPa,
ξ =19.0%), X= 20247.16 MPa %, that > AHSS.

On the contrary, alloying elements in S-52 N Mn steel, have a dominant effect of reaching AHSS, XHSS, and UHSS via ceramization at low energy 220°C for 10 and 30 minutes with boron mix and or boron mix + ABC (Figure 12a-e). Fig.12a. reveals low strength for Seamless AR (σ =1360.85 MPa, ξ =44.0), X=59877.4 MPa %. Fig. 12b, reveals slightly more increase of strength and ductility when ceramized with (Boron Mix only), (σ =1342.71 MPa, ξ =54.00), X=72506.34 MPA %. Fig. 12c, reveals slightly more increase of strength and ductility when ceramized with (Boron Mix + ABC), (σ =1393.69 MPa, ξ =52.50), X=73168 MPa %. Figure 12d, reveals slightly more increase of strength and ductility when ceramized with (Boron Mix only), (σ =1511.6 MPa, ξ =52.5), X=79359 MPa %. Figure 12e, reveals slightly more increase of strength and ductility when ceramized with Boron Mix + ABC (σ =1582.07 MPa, ξ =60.0), X=94924.00 MPa %. That all are > UHSS.

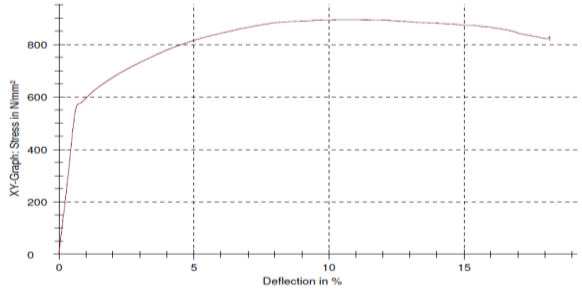

Figure 11.a**.** Seamless AR (σ=895.00 MPa, ξ=18.0%), X= 16110 MPa %.

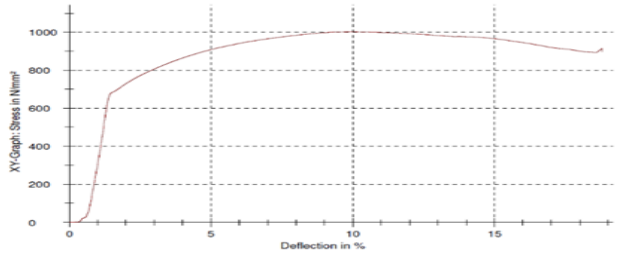

Figure 11.b. Ceramized Seamless (220 °C/10 min (Mix)) 3-point bending (σ=1003.142 MPa, ξ=19.0%), X= 19058.9 MPa %.

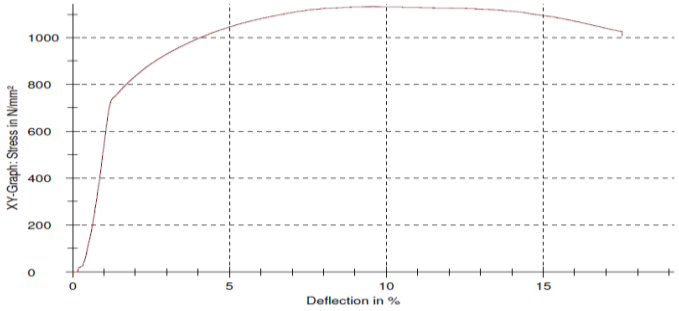

Figure 11.c**.** Ceramized Seamless (220 °C/10 (Mix+ABC)) 3-point bending (σ=1132.42 MPa, ξ=17.5%), X= 19817.35 MPa %.

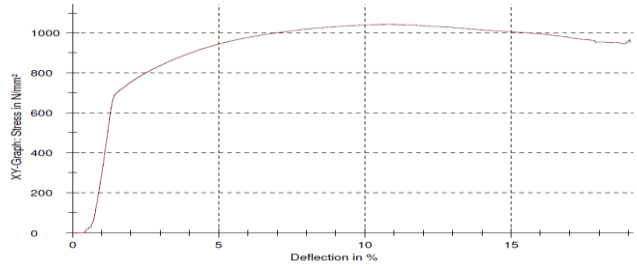

Figure 11.d. Ceramized Seamless (220 °C/30 min (Mix)) 3-point bending (σ=1043.92.42 MPa, ξ=19.0%), X= 19834.48 MPa %.

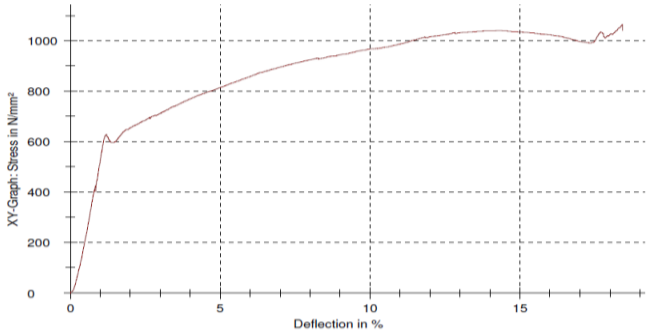

Figure 11.e. Ceramized Seamless (220 °C/30 min (Mix+ABC)) 3-point bending (σ=1065.64 MPa, ξ=19.0%), X= 20247.16 MPa %

Figure 11a-e. 3-point bending test and flexural strength of (a) AR, and (b-e) ceramized / boronized seamless low alloy steel (A333 Gr.6) specimens with its represented values

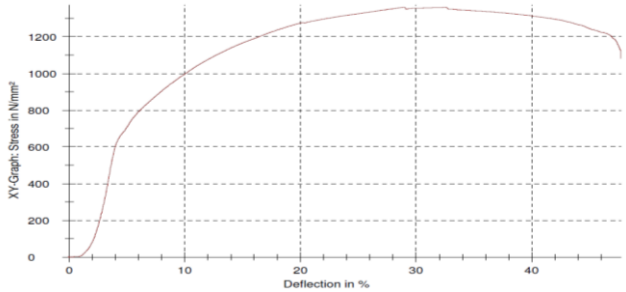

Figure 12.a**.** As Received S-52 N, 3-point bending (σ=1360.85 MPa, ξ=44.0), X=59877.4 MPa %.

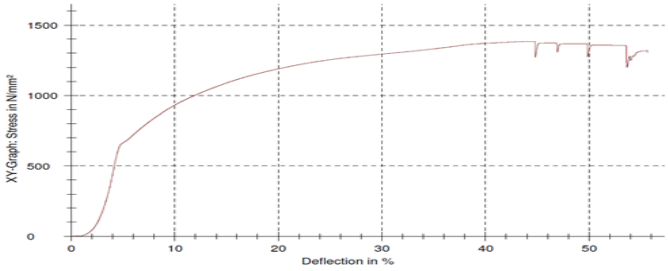

Figure 12.b. 3-Point Bending of Ceramized steel S-52 N, at 220 °C/10 min. (Mix), (σ=1342.71 MPa, ξ=54.00), X=72506.34

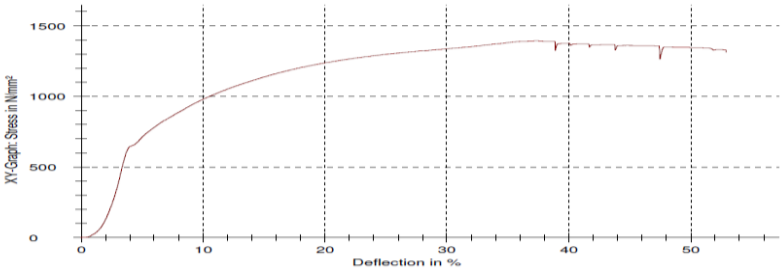

Figure 12.c. 3-Point Bending of Ceramized steel S-52 N, at 220 °C/10 min. (Mix+ABC), (σ=1393.69 MPa, ξ=52.50), X=73168 MPa %.

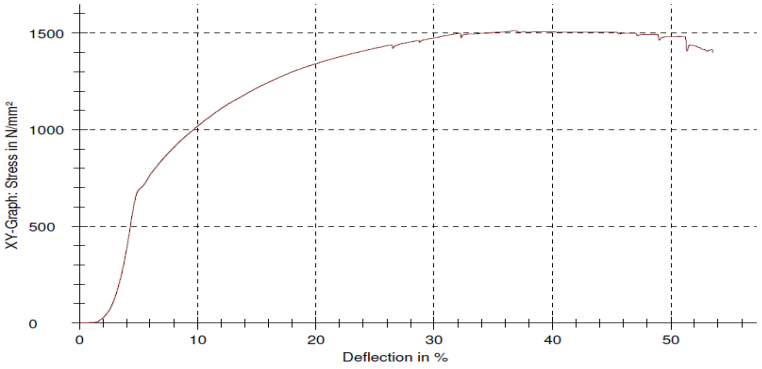

Figure 12.d. 3-Point Bending of Ceramized steel S-52 N, at 220 °C/30 min. (Mix), (σ=1511.6 MPa, ξ=52.50), X=79359 MPa %.

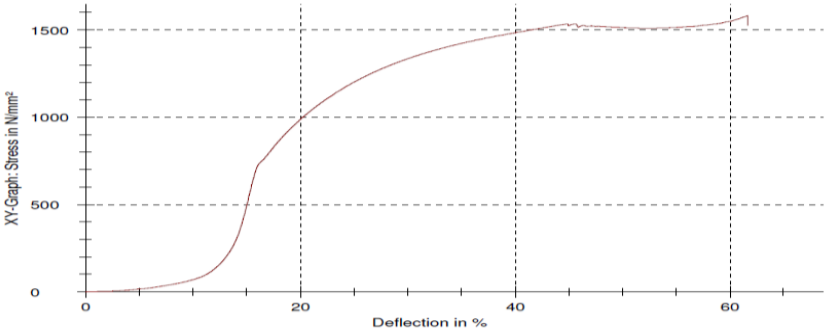

Figure 12.e. 3-Point Bending of Ceramized steel S-52 N, at 220 °C/30 min. (Mix+ABC),

(σ=1582.07 MPa, ξ=60.0), X=94924.00 MPa %.

Figure 12a-e. 3-point bending test and flexural strength of (a) AR, and (b-e) ceramized/ boronized Mn-alloy steel (S52-N) specimens with its represented values.

4. Conclusion

The mechanical properties of as received low alloy steel and Mn alloy steel along with ultra-fast low energy ceramization have been investigated and correlated with microstructural evidence that reveal the kinetic of both thermochemical fusion and thermomechanical processing. The main findings are summarized as follows:

- Kinetic of ceramization is established via scanning electron microscopy (SEM) and energy dispersive x-ray spectroscopy (EDX) as. 1-Localized melting with alloy segregation, 2- phase transformation with stress mismatch, 3-thermite reaction with defragmentation, 4-twinning and recrystallization, 5-chemical and mechanical mesh of ceramic/metal bonding are also acoustically and thermally captured.
- The AR low alloy seamless sample shows advanced high strength with X= 20247.16 MPa %, that $\geq$ AHSS.
- The AR Mn alloy steel (S52-N) sample shows advanced ultra-high strength with X= X=59877.4 MPa %, that $\geq$ XHSS.
- Ceramized Mn steel reveals Ultra high strength steel that established with both boron mix, and more established with boron mix and ammonium bicarbonates (ABC) with X=94924.00 MPa %.
- A synergetic effect of boron and ABC induce more strength more ductility for hybrid structure.

References

[1] Bakr M Rabeeh, Mahmoud M Abu-Elkhair and Mahmoud H Reda 2017 Engineering and in Situ Intrinsically Processing of Boron-Based, Carbon Nano Fiber reinforcement in A Hybrid Composite Implant, Int. Conf. Metall. Technol. Mater. (ICMTM), V. **232**, New York, USA

[2] Liu X C, Zhang H W and Lu K 2013 Strain-induced ultra-hard and ultra-stable Nano-laminated Structure in nickel, Int. Journal of Material Science **342**, 337–340

[3] Koyama M et al 2017 Bone-like crack resistance in hierarchical metastable Nano laminate steels, Int. Journal of Material Science, **355**, 1055–1057

[4] Wat A et al 2019 Bio inspired nacre -like alumina with a bulk-metallic glass forming alloy as a Compliant phase, National Commun. Journal **10**, 1–12

[5] Li X, Wei Y, Lu L, Lu K and Gao H 2010 Dislocation nucleation governed softening and maximum Strength in Nano-twinned metals, Nature Science, **464**, 877–880

[6] Huang C X et al 2018 Interface affected zone for optimal strength and ductility in heterogeneous Laminate, Materials Today **21**, 713–719

[7] An X H et al 2015 Atomic-scale investigation of interface facilitated deformation twinning in severely Deformed Ag-Cu Nano lamellar composites. Appl. Phys. Lett. **107**, 011901

[8] Zheng S et al 2013 High-strength and thermally stable bulk Nano layered composites due to twin-Induced interfaces, National Commun. Journal **4**, 1–8

[9] Gleiter H 1995 Nanostructured materials: state of the art and perspectives, Nanostructure Materials Journal Vol. **6**, 3–14

[10] Koch C C, Morris D G, Lu K and Inoue A 1999 Ductility of nanostructured materials, MRS Bull. **24**, 54–58

[11] Lu Y and Liaw P K 2001The mechanical properties of nanostructured materials. JOM **53**, 31–35
[12] Kumar K S, Van Swygenhoven H and Suresh S 2003 Mechanical behavior of Nano crystalline Metals and alloys, Acta Mater. **51**, 5743–5774
[13] Wei Y et al 2014 Evading the strength-ductility trade-off dilemma in steel through gradient hierarchical Nano twins, National Commun. **5**, 1–8
[14] Li Z, Pradeep K G, Deng Y, Raabe D and Tasan C C 2016 Meta-stable high entropy dual-phase alloys Overcome the strength–ductility trade-off. Nature **534**, 227–230
[15] Lei Z et al 2018 Enhanced strength and ductility in a high-entropy alloy via ordered oxygen complexes, Nature **563**, 546–550
[16] Gludovatz B et al, 2014 A fracture-resistant high-entropy alloy for cryogenic applications, Science Journal Vol. **345**, 1153–1158
[17] Ding Q et al 2019 Tuning element distribution, structure and properties by composition in high-entropy Alloys. Nature **574**, 223–227
[18] Olson G B 1997 Computational design of hierarchically structured materials, Science Journal Vol. **277**, 1237–1242
[19] Lu K, 2014 Making strong Nano materials ductile with gradients, Science Journal, Vol. **345**, 1455–1456
[20] Wang Y, Chen M, Zhou F and Ma E 2002 High tensile ductility in a nanostructured, metal Nature **419**, 912–915
[21] Marwa M S, Bayoumi M A and Bakr M R 2021 Boronizing Mitigate Failure Mechanisms with Extended Life in Oil / Gas Steel Piping Under Acoustic Induced Vibration (AIV). J. Al-Azhar Univ. Eng. Sect., Vol. **16**, PP 252-263
[22] Rabeeh B M 2015 Ultra-fast boriding and surface hardening of low carbon steel, TMS 2015 **14** 4th Annual Meeting and Exhibition, March 15-19, Orlando, FL, USA